Acta Crystallographica Section D
Biological Crystallography
ISSN 0907-4449

The 1.2 Å structure of the human sulfite oxidase cytochrome b_5 domain

Michael J. Rudolph,[a] Jean L. Johnson,[b] K. V. Rajagopalan[b] and Caroline Kisker[a]*

[a]Department of Pharmacological Sciences and Center for Structural Biology, State University of New York at Stony Brook, Stony Brook, New York 11794-5115, USA, and [b]Department of Biochemistry, Duke University Medical Center, Durham, North Carolina 27710, USA

Correspondence e-mail: kisker@pharm.sunysb.edu

Received 21 February 2003
Accepted 6 May 2003

The molybdenum- and iron-containing enzyme sulfite oxidase catalyzes the physiologically vital oxidation of sulfite to sulfate. Sulfite oxidase contains three domains: an N-terminal cytochrome b_5 domain, a central domain harboring the molybdenum cofactor (Moco) and a C-terminal dimerization domain. Oxidation of the substrate sulfite is coupled to the transfer of two electrons to the molybdenum cofactor. Subsequently, these electrons are passed on, one at a time, to the b_5 heme of sulfite oxidase and from there to the soluble electron carrier cytochrome *c*. The crystal structure of the oxidized human sulfite oxidase cytochrome b_5 domain has been determined at 1.2 Å resolution and has been refined to a crystallographic R factor of 0.107 ($R_{\rm free}$ = 0.137). A comparison of this structure with other b_5-type cytochromes reveals distinct structural features present in the sulfite oxidase b_5 domain which promote optimal electron transport between the Moco of sulfite oxidase and the heme of cytochrome *c*.

1. Introduction

Sulfite oxidase catalyzes the terminal step in the degradation of the sulfur-containing amino acids cysteine and methionine and also serves to detoxify sulfite derived from environmental sources (Hille, 1996; Kisker, Schindelin & Rees, 1997). In addition, sulfite oxidase is involved in the direct oxidation of sulfite to sulfate in different phototrophic bacteria (Kappler *et al.*, 2000). Sulfite oxidase in eukaryotes is located in the mitochondrial intermembrane space (Johnson & Rajagopalan, 1976). The crystal structure of chicken sulfite oxidase (CSO) has been determined at 1.9 Å resolution (Kisker, Schindelin, Pacheco *et al.*, 1997). The enzyme is a homodimer with a molecular mass of ~110 kDa and each monomer is divided into three domains. Domain I harbors the b_5 heme and has a molecular mass of ~10 kDa. Domains II and III have a combined molecular mass of ~42 kDa and consist of the molybdenum-cofactor (Moco) domain and an immunoglobulin-like domain which is responsible for dimerization. The enzyme can be separated by limited proteolysis into two fragments (Johnson & Rajagopalan, 1977): an N-terminal fragment harboring the b_5 heme and a C-terminal fragment containing the Moco.

The net reaction catalyzed by sulfite oxidase is the transfer of one O atom from water to the substrate (sulfite). Substrate binding occurs in close spatial proximity to the Moco (Kisker, Schindelin & Rees, 1997); coupled with substrate oxidation, two electrons are transferred from sulfite to the molybdenum

center of the cofactor. The two electrons are subsequently transferred from the Moco to the cytochrome b_5-type heme in a two-step reaction, from where they are donated to the final electron acceptor cytochrome *c* (Fig. 1). A surprising finding in the CSO structure (Kisker, Schindelin & Rees, 1997) was the arrangement of the cytochrome b_5 domain relative to the remainder of the enzyme, which was characterized by a large distance (32 Å) between the metals in the Moco and heme. The measured electron-transfer rates are too large given the donor–acceptor distance observed in the crystal structure and conformational changes have been postulated that bring the cytochrome b_5 domain into close proximity to the Moco (Feng *et al.*, 2002; Pacheco *et al.*, 1999).

In order to better understand the process of electron transfer in sulfite oxidase, we have determined the three-dimensional structure of the human sulfite oxidase b_5 domain (HSO b_5) in the oxidized state at 1.2 Å resolution and compared it with the b_5 domain of chicken sulfite oxidase (CSO b_5; Kisker, Schindelin & Rees, 1997) and bovine cytochrome b_5 (CYT b_5; Durley & Mathews, 1996). The high-resolution structure of HSO b_5 reveals features which explain its altered redox potential when compared with CYT b_5. These studies contribute to an understanding of the role of the b_5 domain in the electron-transfer steps during the sulfite oxidase-catalyzed redox reaction.

2. Methods

2.1. Expression and purification of human sulfite oxidase

His-tagged human sulfite oxidase (HSO) was expressed in *Escherichia coli* TP1000 cells containing pTG718 as described by Temple & Rajagopalan (2000). After harvesting, the cells were lysed in the presence of a mixture of protease inhibitors supplied as EDTA-free protease-inhibitor cocktail tablets (Roche Diagnostics). Chromatography on Ni–NTA resin was carried out as described in Temple & Rajagopalan (2000) and was followed by a final purification step on DE-52 using a gradient of sodium phosphate buffer pH 7.8 from 50 to 350 m*M* containing 0.1 m*M* EDTA.

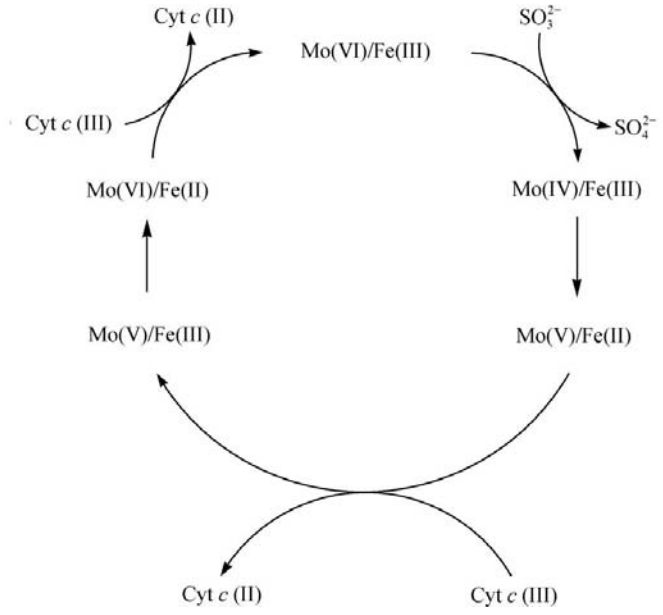

Figure 1
Sulfite oxidase-catalyzed reaction. The reaction consists of the oxidation of sulfite to sulfate coupled with the subsequent reduction of two equivalents of ferricytochrome *c* to ferrocytochrome *c*.

2.2. Generation of a human sulfite oxidase homology model

A molecular model of the HSO Moco and dimerization domains was generated with the program *SWISS-PDB Viewer* (Guex & Peitsch, 1997) based on the structure of CSO (Kisker, Schindelin & Rees, 1997). CSO displays 62% sequence identity in the Moco domain and 44% in the dimerization domain. Amino acids 90–467 from HSO were aligned with CSO residues 90–466 and residues in the crystal structure of CSO (PDB code 1sox) were replaced with the corresponding residues of HSO. The resulting model was energy-minimized to optimize the stereochemistry and to remove any steric clashes between adjacent atoms.

2.3. Crystallization of HSO b_5, structure determination and refinement

The HSO b_5 domain was inadvertently crystallized in crystallization setups for full-length HSO. The b_5 fragment was formed spontaneously from intact HSO by proteolytic degradation and selectively crystallized from the mixture by vapor diffusion from a 1:1 ratio of HSO at 10 mg ml^{-1} and a reservoir solution containing 1.5 *M* $(NH_4)_2SO_4$, 0.1 *M* Tris pH 8.5. The crystals had a red-brown color and grew to dimensions of 0.4 × 0.3 × 0.1 mm. The crystals belong to space group *C*2, with unit-cell parameters a = 98.9, b = 35.4, c = 26.3 Å, β = 93.8°. Given the unit-cell parameters, there is one molecule in the asymmetric unit, resulting in a Matthews coefficient (V_M) of 2.6 Å^3 Da^{-1}. Diffraction data were collected from cryocooled crystals soaked in mother liquor containing 25%(*v*/*v*) glycerol. Diffraction data were collected at a wavelength of 1.1 Å at beamline X26C at the National Synchrotron Light Source (NSLS) at Brookhaven National Laboratory. Data were indexed, integrated and scaled using *HKL* (Otwinowski & Minor, 1997). The structure was solved by molecular replacement using the CSO b_5 domain (Kisker, Schindelin & Rees, 1997) as the search model (PDB code 1sox). The rotational and translational searches were performed using the program *AMoRe* (Navaza, 1994), with data in the resolution range 8–3.5 Å. Molecular replacement resulted in an initial *R* factor of 0.489 and a correlation coefficient of 0.333. The initial phase information was used to calculate electron-density maps, which were used to build a model of residues 3–82 of HSO b_5 using the program *O* (Jones *et al.*, 1991). For subsequent calculations the *CCP*4 suite was utilized (Collaborative Computational Project, Number 4, 1994). Refinement of the model was performed using *REFMAC*5 (Murshudov *et al.*, 1997) with amplitudes to 1.2 Å resolution, including refinement of anisotropic temperature factors and incorporation of H atoms in their riding positions.

Table 1
Data-collection statistics.

Values in parentheses refer to the highest resolution data shell.

Maximum resolution (Å)	1.20
Redundancy	2.2
Observed reflections	63140
Unique reflections	28384
Completeness (%)	96.0 (88.0)
$R_{\rm sym}$† (%)	8.9 (27.0)
$\langle I\rangle/\langle\sigma(I)\rangle$‡	12.9 (1.7)

† $R_{\rm sym} = \sum_{hkl}\sum_i |I_i - \langle I\rangle|/\sum_{hkl}\sum_i I_i$, where I_i is the ith measurement and $\langle I\rangle$ is the weighted mean of all measurements of I. ‡ $\langle I\rangle/\langle\sigma(I)\rangle$ indicates the average of the intensity divided by its standard deviation.

The program *ARP* (Perrakis *et al.*, 1999) was used to add water molecules to the resulting density maps. The structure of HSO b_5 was compared with the structures of CSO b_5 (PDB code 1sox) and CYT b_5 (PDB code 1cyo).

3. Results and discussion

3.1. Structure of HSO b_5 domain

During crystallization of full-length HSO spontaneous proteolysis generated a fragment consisting of its cytochrome b_5 domain, the structure of which is described here. No attempts were made to define the C-terminal boundary of this fragment by mass spectrometry. The data set used for structure analysis contained 28 384 unique reflections obtained from a total of 63 140 recorded reflections in the resolution range 50–1.2 Å. The overall completeness and $R_{\rm sym}$ were 96.0 and 8.9%, respectively, with values of 88.8 and 27.0% in the highest resolution shell (Table 1). The crystal structure of HSO b_5 was solved by molecular replacement and refined at 1.2 Å resolution to an R factor of 0.107 ($R_{\rm free}$ = 0.137), including anisotropic temperature factors. For comparison, the same model refined with isotropic temperature factors yields an R factor of 0.155 ($R_{\rm free}$ = 0.183). The simultaneous decrease in both the crystallographic R factor and the free R factor upon refinement of anisotropic temperature factors by 4.8 and 4.6%, respectively, clearly justifies this refinement approach. H atoms in riding positions were included during the refinement, leading to a decrease in the R factor of 1.1% and in $R_{\rm free}$ of 1.3%.

Table 2
Molecular replacement and refinement statistics.

Molecular replacement	
Initial R factor	0.489
Correlation coefficient†	0.333
Resolution range (Å)	8.0–3.5
Refinement	
Resolution range (Å)	10–1.2
No. of reflections‡	26112
Data-to-parameter ratio	1.7
No. of protein/hetero/solvent atoms	1529/48/120
$R_{\rm cryst}$ ($R_{\rm free}$)§	0.107 (0.137)
Deviations from ideal values in	
Bond distances (Å)	0.023
Bond angles (°)	2.18
Planar 1,4 distances (Å)	0.013
Chiral volumes (Å^3)	0.150
Torsion angles (°)	3.58
van der Waals repulsion (Å)	0.32
Ramachandran statistics¶	0.938/0.062
B factor (Å^2)	
Main chain	18.0
Side chains	17.6
Overall	17.9
Overall coordinate error†† (Å)	0.03

† Correlation coefficient between the observed and calculated structure-factor amplitudes after molecular replacement and rigid-body refinement. ‡ Number of reflections used during the refinement process. § $R_{\rm cryst} = \sum_{hkl}\big||F_o| - |F_c|\big|/\sum_{hkl}|F_o|$, where F_o and F_c are the observed and calculated structure-factor amplitudes, respectively. $R_{\rm free}$ is the same as $R_{\rm cryst}$ for 5% of the data randomly omitted from refinement. ¶ Ramachandran statistics indicate the fraction of residues in the most favored and additionally allowed regions of the Ramachandran diagram as defined by *PROCHECK*. No residues are in disallowed regions. †† Data-precision index (Cruickshank, 1999) estimated from $R_{\rm free}$ as determined by *REFMAC*.

The overall quality of the electron-density maps is excellent (Fig. 2) as corroborated by the crystallographic and free R factors. The Ramachandran diagram has 93.8% of the residues in the most favored region and 6.2% in additionally allowed regions (Table 2). The final model contains residues 3–82 with dual alternate conformations for residues Glu11, Val37 and Leu61, the heme prosthetic group, 122 water molecules, one sulfate and one glycerol molecule. At the N-terminus, residues 1–2 appear to be disordered and there are presumably additional disordered residues at the C-terminus, but owing to the spontaneous nature of the proteolytic event their number is unknown.

The fold of HSO b_5 (Fig. 3) is composed of a mixed $\alpha+\beta$ architecture with a central four-stranded antiparallel β-sheet (β1–β4), one α-helix (helix 1) on one side of the sheet and three α-helices (helices 3, 4 and 6) and two 3_{10}-helices (helices 2 and 5) on the opposite side of the β-sheet. The β-sheet along with five helices (helices 2–6) forms a

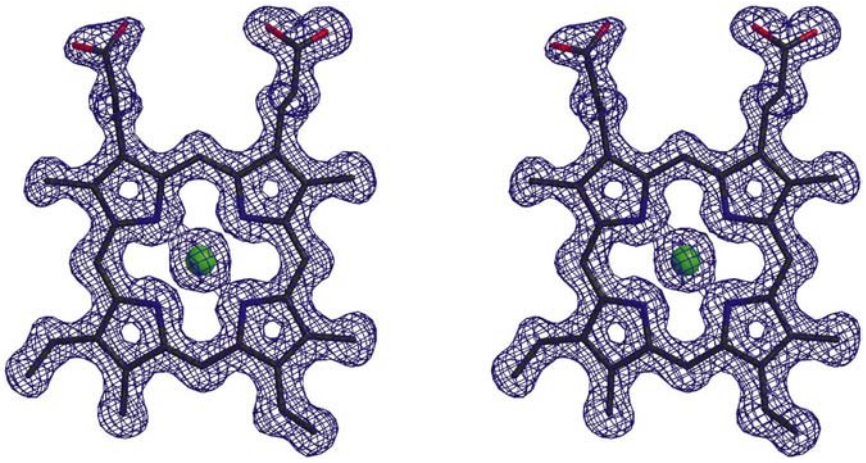

Figure 2
σ_A-weighted $2F_o - F_c$ electron-density map at 1.2 Å surrounding an all-bonds representation of the heme cofactor contoured at 1σ. The heme has both propionate groups in a fully extended conformation. The Fe atom is colored green. Figs. 2, 3, 8, 9(*a*) and 9(*c*) were generated with *MOLSCRIPT* (Kraulis, 1991) and *Raster3D* (Merritt & Bacon, 1997).

cavity that grasps the heme. Although the heme is not covalently attached to the protein, it is firmly encapsulated in this hydrophobic cleft. The heme vinyl groups face towards the hydrophobic core of the protein and the two extended propionate side chains face towards the solvent. The heme iron is octahedrally coordinated by the $N^{\varepsilon 2}$ atoms of the axial histidines at positions 40 and 65 at a distance of 1.99 Å and the four pyrrole ring N atoms at 2.00, 1.99, 2.03 and 1.94 Å, respectively. Almost identical distances (within 0.01 Å) were obtained irrespectively of whether or not the metal–ligand distances were restrained during refinement. The ligand distances bear considerable validity, as the overall coordinate error is predicted to be only ∼0.03 Å based on the data-precision index (Cruickshank, 1999) as calculated by *REFMAC*.

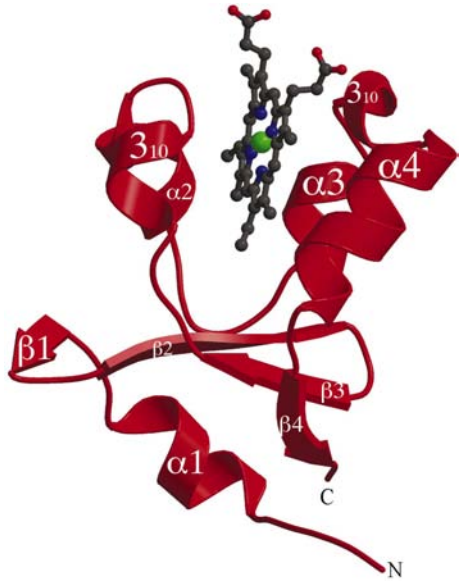

Figure 3
Ribbon diagram of HSO b_5 colored in red. The heme is shown in ball-and-stick representation, with the iron in green. Secondary-structure elements and the N- and C-termini are labeled.

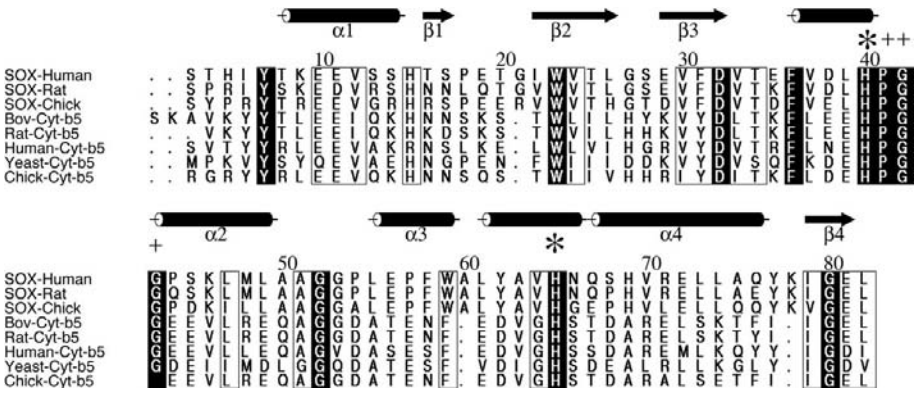

Figure 4
Primary sequence alignment of eight members of the cytochrome b_5 family. Identical and conserved residues are highlighted in black and enclosed in a box, respectively. His40 and His65, the strictly conserved iron ligands, are highlighted by an asterisk. The Pro41-Gly42-Gly43 motif is highlighted by plus signs. Secondary-structure elements determined with *PROMOTIF* are indicated. Figure generated with *ALSCRIPT* (Barton, 1993).

3.2. Structural comparison of cytochrome b_5 domains

The primary sequence identity between HSO b_5 and CSO b_5 is 83%, while that between HSO b_5 and CYT b_5 is 42% (Fig. 4). The structural similarity is also evident, as the superposition of 80 equivalent C^{α} atoms of HSO b_5 onto CSO b_5 results in an overall root-mean-square (r.m.s.) deviation of 0.81 Å. The r.m.s. deviation drops to 0.65 Å after the removal of residues 3 and 4, which possess the largest coordinate displacements of 3.0 and 2.8 Å, respectively. The superposition of HSO b_5 onto CYT b_5 yields an overall r.m.s. deviation of 1.37 Å for 77 equivalent C^{α} atoms. Thus, as expected, HSO b_5 is clearly a member of the cytochrome b_5 superfamily and is most closely related to the b_5 domain of CSO. Each of the proteins within this family retains the $\alpha+\beta$ fold, although HSO b_5 contains an antiparallel β-sheet with only four β-strands instead of the five found in CSO b_5. HSO b_5 contains the same six helices as CSO b_5, although two of the helices have been modified to 3_{10}-helices in HSO b_5. The deviations in helical periodicity may be attributable to crystal contacts, since only two amino-acid differences are noted within the helices themselves. In contrast, of the six helices found in HSO b_5 only four are present in CYT b_5, with the 3_{10}-helices being absent.

All members of the cytochrome b_5 family, including the structurally characterized HSO b_5, CSO b_5 and CYT b_5, exhibit a Pro-Gly-Gly motif (residues 41–43 in HSO b_5) at the top of the cleft which enhances the solvent exposure of the heme propionate located on the *D* ring. The proline causes a kink in the peptide chain away from the heme group and the two Gly residues provide a large opening which exposes the *D* propionate. This solvent-exposed propionate has been implicated in protein–protein interactions (Durham *et al.*, 1995) and in regulation of the redox potential of cytochrome b_5 (Rivera *et al.*, 1998).

Interactions between CSO b_5 and its electron donor, the Moco domain of CSO, as observed in the crystal structure of CSO (Kisker, Schindelin & Rees, 1997), are primarily hydrophobic in nature and produce a large molybdenum-to-heme distance of 32 Å. This distance is expected to yield much slower electron-transfer rates of $<100\ s^{-1}$ in contrast to the measured rate for CSO of $\sim 1000\ s^{-1}$ (Pacheco *et al.*, 1999). Models resulting in a closer Moco-to-heme distance have been proposed (Pacheco *et al.*, 1999) that emphasize the importance of electrostatic interactions between the Moco and cytochrome b_5 domains (Fig. 5). The electrostatic surfaces of the respective molecules within this electron-transfer system demonstrate a mechanism for specificity by way of the electrostatic complementarity between HSO b_5 and the HSO Moco domain as derived from the molecular model. Similar electrostatic features are also present in

CSO b_5 and the CSO Moco domain. Specifically, a prominent electropositive surface surrounding the active site of the Moco domain and the electronegative surface encasing the heme in HSO b_5 (Fig. 6) would support a closer approach of both redox centers, thus facilitating electron transfer from the Moco to the b_5 heme. The proposed interaction would bring the Moco and heme to within a distance of ~12 Å as suggested by manual docking studies. This geometry would be compatible with the distances between cofactors typically observed in electron-transfer proteins (Page *et al.*, 1999), producing a more rapid electron-transfer rate which is compatible with the observed electron-transfer rate of $\sim 10^3\ s^{-1}$ between the Moco and heme groups. Subsequently, the complementarity of the oppositely charged surfaces of cytochrome *c* and HSO b_5 (Fig. 6) would lead to the production of an activated complex with a distance of ~9 Å between the two heme molecules according to manual docking studies. This distance is consistent with the experimentally observed electron-transfer rates of $\sim 10^5\ s^{-1}$ for the cytochrome b_5–cytochrome *c* complex (Durham *et al.*, 1995).

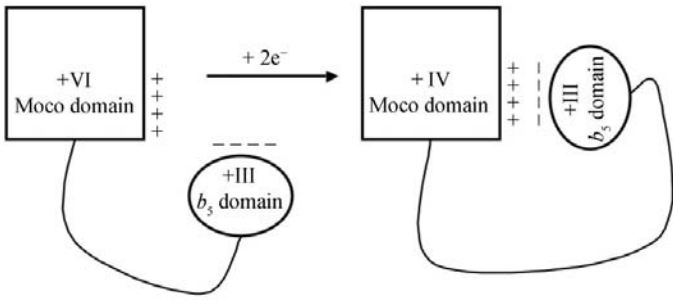

Figure 5
Schematic view of the proposed conformational change moving the Moco and b_5 domains closer to each other during the electron-transfer process after the substrate, sulfite, has been oxidized to sulfate in a two-electron-transfer reaction. Note the positively charged region surrounding the Moco domain active site and the negatively charged region neighboring the b_5 domain active site represented by plus and minus signs, respectively. The Moco domain is in the +VI oxidation state and is reduced to the +IV state subsequent to the two-electron oxidation of the substrate sulfite. Furthermore, the b_5 domain is in the +III oxidation state and can accept one electron at a time from the Moco domain.

3.3. Impact of protein structure on heme redox potential

The redox potentials of heme-containing proteins span a range of about −400 to +400 mV (Rees, 1985). Since the redox potential is influenced by the microenvironment provided by the three-dimensional structure of the protein, different ligand environments can result in tremendous variations in the redox potential of a prosthetic group. The midpoint potentials of HSO b_5 and CYT b_5 are 50 mV (Hille, 1996) and −100 mV (Altuve *et al.*, 2001), respectively. A comparison of the crystal structures of HSO b_5 and CYT b_5, as outlined in the following sections, reveals specific structural elements which are consistent with the higher redox potential of the heme in HSO b_5.

3.3.1. Comparison of cytochrome b_5 cavities. HSO b_5, CSO b_5 and CYT b_5 differ slightly in the dimensions of their heme cavities. HSO b_5 and CSO b_5 have very similar cavity volumes of 679 and 712 $Å^3$, respectively, while CYT b_5 has a somewhat larger volume of 795 $Å^3$. The buried surface areas upon heme binding of 1101, 1063 and 1009 $Å^2$ for HSO b_5, CSO b_5 and CYT b_5, respectively, suggest a somewhat tighter heme binding in the sulfite oxidase b_5 domains compared with CYT b_5. The differences in cavity volumes and surface-binding areas define differences in the microenvironments of the respective heme molecules and affect the redox potentials. The sulfite oxidase b_5 domains exhibit higher redox potentials than CYT b_5 as would be expected, since exclusion of solvent

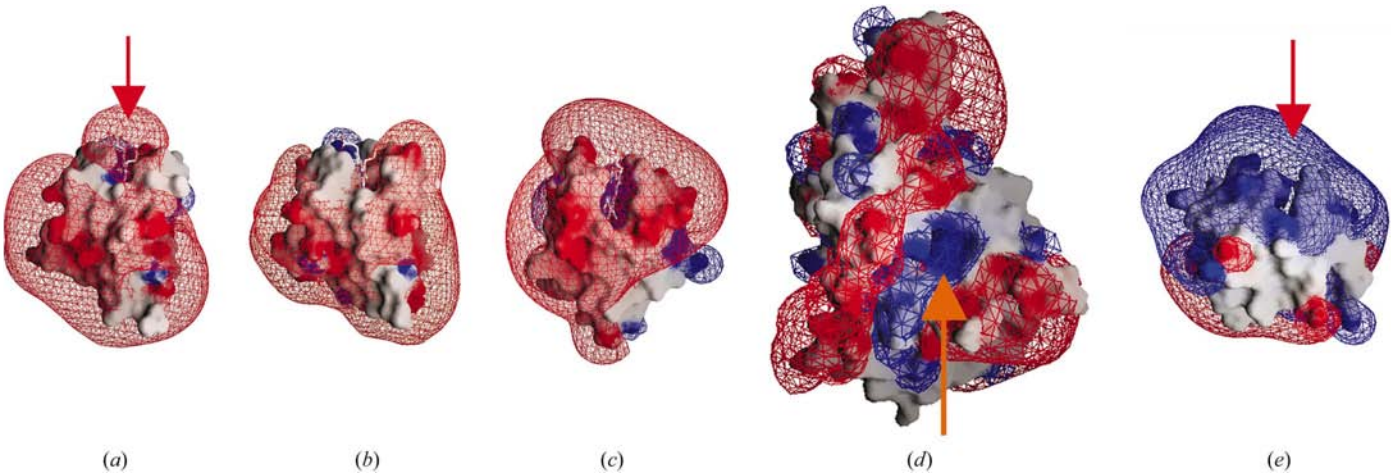

Figure 6
Electrostatic surface and isopotential contour representation of (*a*) HSO b_5, (*b*) CSO b_5, (*c*) CYT b_5, (*d*) the homology model of the HSO Moco domain and (*e*) cytochrome *c* (PDB code 2ycc). Blue and red regions representing electropositive ($>7k_BT$) and electronegative ($<-7k_BT$) potential, respectively, are mapped onto the molecular surfaces. Isopotential contours at $\pm 1k_BT$ are drawn where the blue and red contour maps represent positive and negative isopotentials. The calculation assumed an ionic strength of 100 m*M*. Note the positive potential around the active site of the HSO Moco domain homology model and the extremely positive isopotential contour above cytochrome *c*. Both surfaces are complementary to HSO b_5. The arrow in the HSO Moco domain model depicts the active site, while the arrows in HSO b_5 and cytochrome *c* point to the heme exposed edges. Figs. 6 and 7 were generated with *GRASP* (Nicholls *et al.*, 1991).

destabilizes the more charged oxidized form. Furthermore, the increased solvent exposure of the CYT b_5 heme may also permit greater heme isomerization (Banci *et al.*, 2000), which would be important in interactions of CYT b_5 with its various substrates. These include the structurally diverse proteins fatty acid desaturase, cytochrome P450 and methemoglobin (Vergeres & Waskell, 1995). The tighter cavity of the sulfite oxidase b_5 domain may impose specificity, restricting interactions to the Moco within the Moco domain as the electron donor and cytochrome *c* as the electron acceptor.

The differences in solvent accessibility of the heme groups of HSO b_5 and CYT b_5 are illustrated in Fig. 7. In HSO b_5 the bulky residues Phe58 and Tyr62 block solvent access, which is much less restricted in CYT b_5 with Asn and Val at the corresponding positions. The partial covering of the HSO b_5 heme group reduces the dielectric constant in the heme environment. The precise increase in the redox potential of HSO predicted by the decreased solvent exposure is difficult to quantify. However, in a study by Wu *et al.* (2000), a mutation of CYT b_5 (Val61His) produced a redox potential augmentation of +21 mV which was attributed to a reduction in the solvent exposure of the heme group.

3.3.2. Comparison of the cytochrome b_5 axial histidine environment. Cytochrome b_5 is a bis-imidazole-coordinated heme. The orientation of the axial histidine ligands relative to the iron and changes in the hydrogen-bond network to these ligands affect the observed redox potential (Sarma *et al.*, 1997). HSO b_5, CSO b_5 and CYT b_5 have similar axial histidine coordinations. A most noticeable conserved feature in all three proteins is the hydrogen bond between each axial histidine $N^{\delta1}$ nitrogen and a main-chain carbonyl O atom. Additional stabilization is provided by stacking either large aromatic side chains (Trp59 in HSO b_5 or Phe58 in CYT b_5) or bulky aliphatic side chains (Ile47 in HSO b_5 or Leu46 in CYT b_5) below each axial histidine.

A notable difference between the axial histidines of HSO b_5 and those of CYT b_5 is their coplanar nature in HSO b_5 in contrast to a ~40° deviation from planarity in CYT b_5 (Fig. 8). This difference appears to arise from a change in the hydrogen-bonding

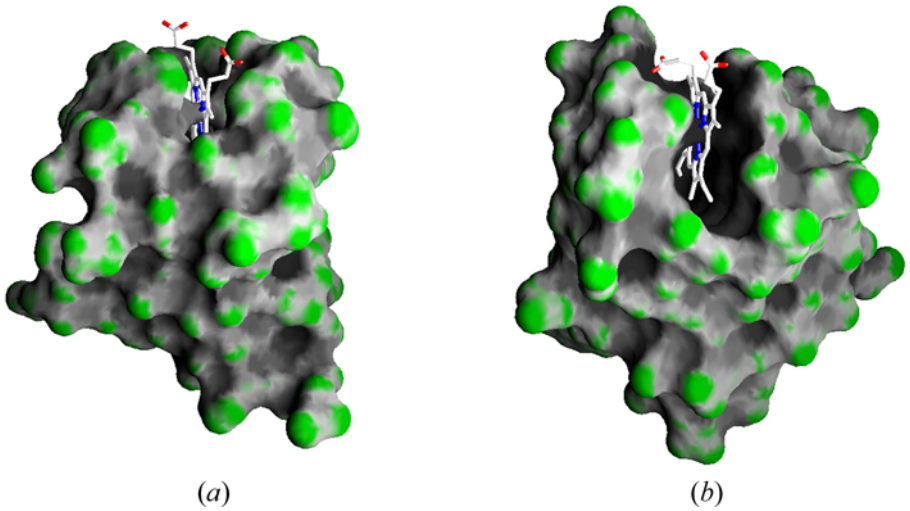

Figure 7
Molecular-surface curvature representations of (*a*)HSO b_5 and (*b*) CYT b_5. Green regions indicate convex sections and gray areas represent concave sections. The heme is shown in an all-bonds representation.

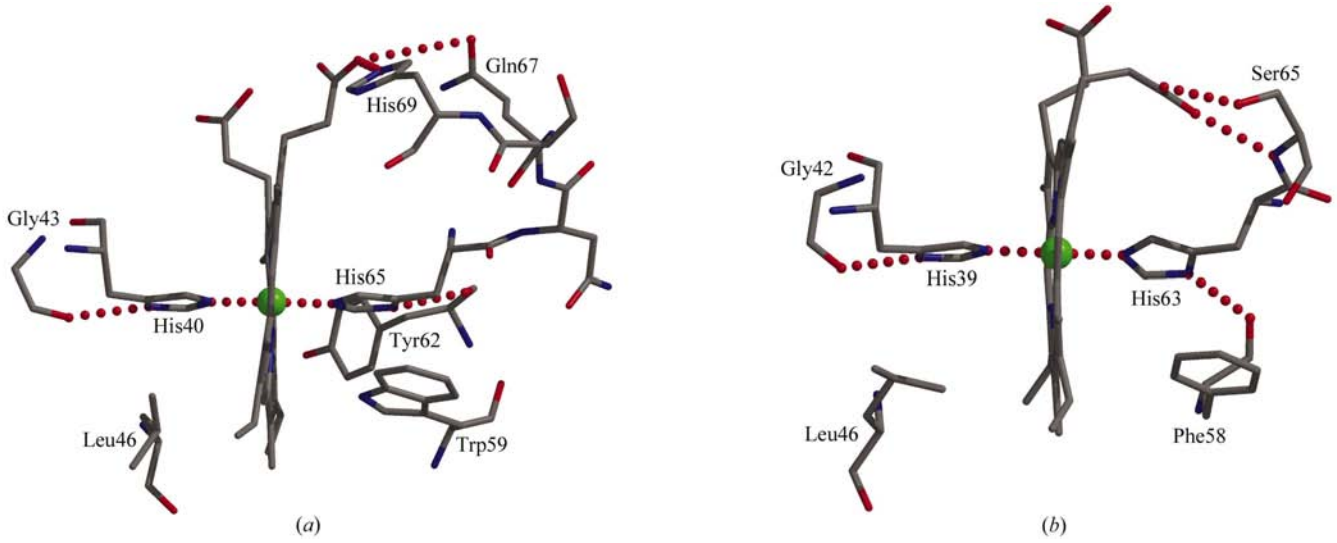

Figure 8
Representation of the HSO b_5 (*a*) and CYT b_5 (*b*) heme axial ligand environments. The heme is shown in all-bonds representation, with the iron in green. The axial histidines are in all-bonds representation, with the red dots depicting the interactions between the Fe atom and the $N^{\varepsilon2}$ atoms of the axial histidines as well as the hydrogen bonds between the carbonyl O atoms and the $N^{\delta1}$ atoms from the axial histidines.

pattern between His65 in HSO b_5 (His63 in CYT b_5) and the main chain. The $N^{\delta1}$ atom of His63 in CYT b_5 forms a hydrogen bond to the carbonyl O atom of Phe58 which is underneath His63, causing the imidazole ring to rotate towards this carbonyl O atom and out of coplanarity with His39. In HSO b_5, the corresponding axial histidine $N^{\delta1}$ nitrogen (His65) forms a hydrogen bond to the carbonyl O atom of Tyr62, which is level with His65, leaving the imidazole ring of His65 coplanar with His40, the other axial ligand. The deviation from coplanarity in CYT b_5 should promote an increase in redox potential, since perpendicularly arranged axial histidines exhibit a 50 mV higher redox potential than coplanar histidines (La Mar & Walker, 1972). However, other structural features counteract this effect such that the net result is an increased potential for HSO b_5 as described in the previous and following sections.

3.3.3. Enthalpic effects on redox potential. If the conformation of an electron-transfer protein is different in the oxidized and reduced states, protein conformation can affect the stability of both oxidation states and therefore influence redox potential (Funk *et al.*, 1990). For example, if a heme protein maintains propionate side chains distant from the heme in the oxidized state, the oxidized state will be destabilized and the redox potential will increase. In the HSO b_5 structure, two hydrogen bonds are formed between the $N^{\varepsilon2}$ atoms of the conserved residues Gln67 and His69 and propionate *A* from the heme group. These extend the propionate away from the heme and destabilize the oxidized state. In contrast, propionate *A* of CYT b_5 forms one main-chain and one side-chain hydrogen bond with Ser64, allowing propionate *A* to bend towards the heme (Fig. 8*b*), stabilizing

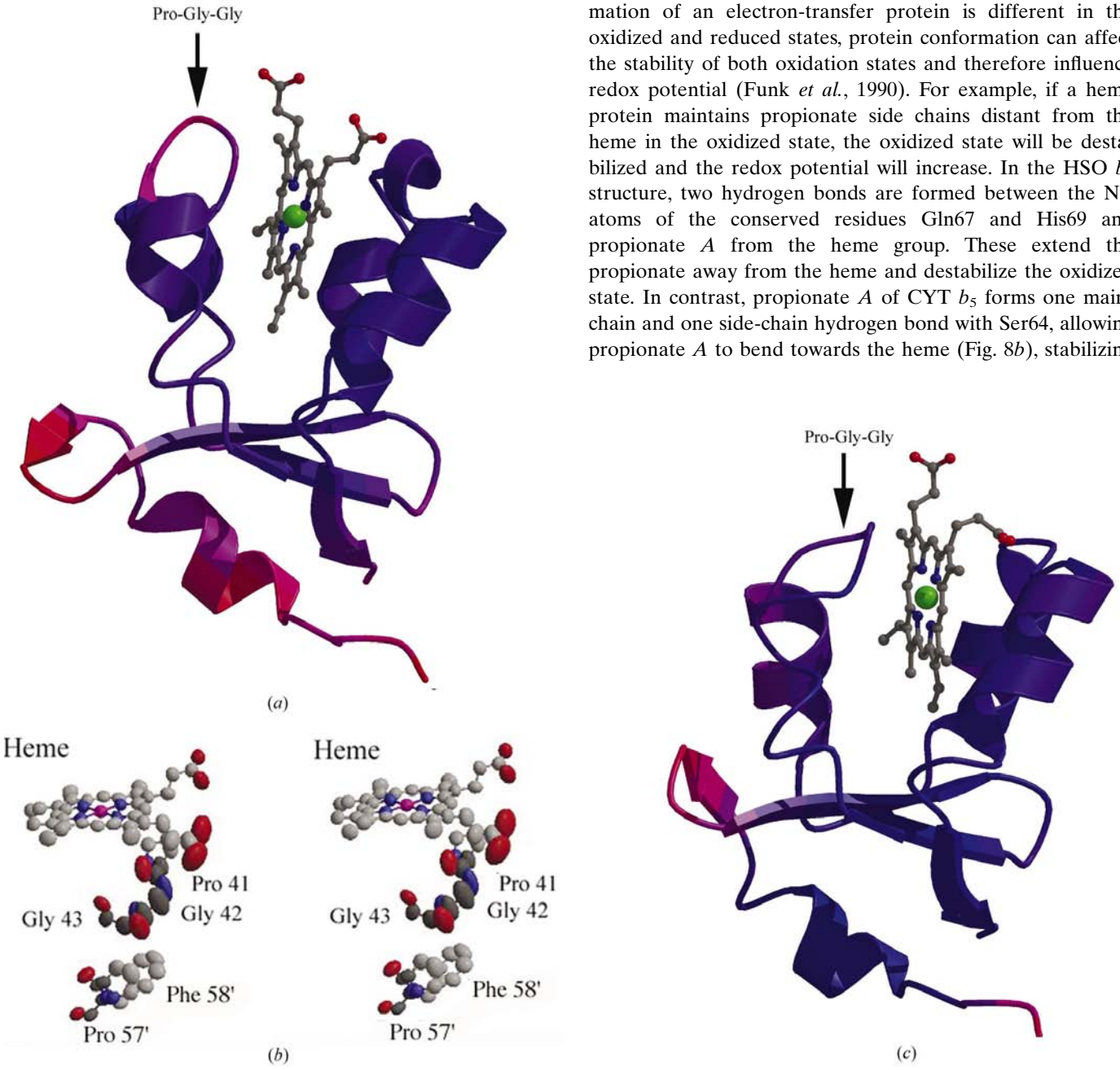

Figure 9
(*a*) Ribbon diagram of the HSO b_5 domain colored according to temperature factors. Blue represents lower temperature factors and red higher temperature factors. The three residues Pro41, Gly42 and Gly43 with relatively high temperature factors are highlighted by the arrow. The heme is displayed in ball-and-stick representation with the Fe atom in green; the N- and C-termini are labeled. (*b*) Ellipsoid stereo representation of the anisotropic temperature factors of Pro41, Gly42, Gly43 and the heme and of Pro57 and Phe58 from a symmetry-related molecule. Gly42 and Gly43 display strong anisotropic motion, whereas the surrounding atoms in the heme and symmetry-related residues display mostly isotropic motion. The ellipsoids are contoured at a probability value of 50%. Fig. 9(*b*) was created with *ORTEP*III (Burnett & Johnson, 1996) and *Raster3D*. (*c*) Ribbon diagram of CYT b_5 color-coded according to temperature factors as described in (*a*), with Pro40, Gly41 and Gly42 highlighted by the arrow.

the oxidized state and lowering the redox potential. Funk *et al.* (1990) have established that the CYT b_5 Ser64Ala mutation resulted in a 7 mV decrease in redox potential, suggesting that the side-chain hydrogen bond may contribute approximately 7 mV towards the difference in the redox potentials.

An additional feature of HSO b_5 that supports a higher redox potential is the electrostatic surface potential surrounding the heme. Although HSO b_5 and CYT b_5 possess a similar overall charge, their surface potentials deviate significantly (Fig. 6). A large negative isopotential is evident on the surface region of CYT b_5 that encompasses the exposed edge of the heme. This negative patch may inhibit the transfer of electrons, as well as force the propionate groups to cluster near the iron, thus stabilizing the oxidized state and efficiently lowering the redox potential. In HSO b_5, the top edge of the molecule displays a significantly smaller negative isopotential contour, as well as a small positive isopotential area. Together, these two features increase the redox potential of HSO b_5 by sequestering the negatively charged propionate side chains away from the heme group.

3.3.4. Entropic effects on redox potential. Entropic effects also influence the redox potential within the b_5 family (Marcus & Sutin, 1985; Blankman *et al.*, 2000). The hydrophobic environment of the b_5 domain displaces solvent surrounding the heme, thus reducing the dielectric constant and increasing the repulsive effect that the oxidized paramagnetic iron has on the surrounding hydrophobic residues. Displacement of the hydrophobic residues adjacent to the oxidized heme initiates a relaxation within the protein, resulting in a significant increase in entropy. This relaxation destabilizes the oxidized state and increases the redox potential.

Analysis of the HSO b_5 structure reveals moderately high temperature factors within the loop region between helices 2 and 3 (Fig. 9*a*), which is very close to the *D* ring of the heme. The overall main-chain temperature factor of HSO b_5 is 13.9 Å^2, while residues 41, 42 and 43 display main-chain temperature factors of 16.9, 26.7 and 17.6 Å^2, respectively. High crystallographic temperature factors can result from either dynamic disorder produced by intrinsic flexibility of the atoms within the molecule or from static disorder in which residues adopt two or more alternate conformations. Residues 40–45 are within a region that exhibits considerable motion in other b_5 cytochromes and contributes significantly to the entropic effect on the redox potential of the rat cytochrome b_5 domain (Dangi *et al.*, 1998). Residues 41–43 of HSO b_5 are dynamically disordered; even at 1.2 Å resolution no discrete conformations can be resolved. The temperature factors in this region are high in spite of the fact that these residues are involved in crystal packing, which should lower the mobility and reduce the temperature factors (Kossiakoff *et al.*, 1992). The distribution of the anisotropic temperature factors in HSO b_5 were examined with the program *PARVATI* (Merritt, 1999) and a normal anisotropism ratio ($E_{\rm min}/E_{\rm max}$) of 0.58 was obtained. A value of 1.0 describes a perfectly isotropic atom and a value of 0 corresponds to a completely anisotropic atom (Merritt, 1999). Gly42 and Gly43 have the highest anisotropy of all main-chain atoms in HSO b_5 (Fig. 9*b*). In contrast, the residues involved in crystal-packing interactions with residues 41–43 do not display significant anisotropy. Together, the elevated temperature factors and the apparently uncorrelated independent anisotropy of residues 41–43 are indicative of dynamic disorder. Consequently, this disordered region should effectively increase the redox potential of HSO b_5. The corresponding residues in CYT b_5 show no significantly elevated temperature factors (Fig. 9*c*) compared with the rest of the protein, indicating that these residues are well ordered and should contribute to the reduced redox potential observed in CYT b_5. The CYT b_5 structure was not refined with anisotropic temperature factors owing to the more limited resolution of 1.5 Å making a more detailed comparison impossible.

4. Conclusions

The atomic resolution structure of HSO b_5 allows a detailed analysis of how the structural features of this domain relate to its function during electron transfer from the Moco to the final electron acceptor cytochrome *c*. A comparison of HSO b_5 and CYT b_5 reveals structural variations that impose enthalpic and entropic effects on the redox potentials of their heme centers. These structural deviations and differing redox potentials enhance the interaction with their specific redox-partner proteins. The variations between HSO b_5 and CYT b_5 direct the selection of the most thermodynamically suitable donor/acceptor molecule, thus optimizing high specificity, as well as electron flux, in order to meet the great demands that biological systems put on electron-transfer proteins.

We thank Ralph D. Wiley for assistance with protein purification and Dr Dieter Schneider for excellent technical support at beamline X26C at the NSLS. This work was supported by grants GM44283 (KVR) and GM58190 (CK) from the National Institutes of Health.

References

Altuve, A., Silchenko, S., Lee, K. H., Kuczera, K., Terzyan, S., Zhang, X., Benson, D. R. & Rivera, M. (2001). *Biochemistry*, **40**, 9469–9483.
Banci, L., Bertini, I., Rosato, A. & Scacchieri, S. (2000). *Eur. J. Biochem.* **267**, 755–766.
Barton, G. J. (1993). *Protein Eng.* **6**, 37–40.
Blankman, J. I., Shahzad, N., Dangi, B., Miller, C. J. & Guiles, R. D. (2000). *Biochemistry*, **39**, 14799–14805.
Burnett, M. N. & Johnson, C. K. (1996). *ORTEP*III. Report ORNL-6985. Oak Ridge National Laboratory, Tennessee, USA.
Collaborative Computational Project, Number 4 (1994). *Acta Cryst.* D**50**, 760–763.
Cruickshank, D. W. (1999). *Acta Cryst.* D**55**, 583–601.
Dangi, B., Blankman, J. I., Miller, C. J., Volkman, B. F. & Guiles, R. D. (1998). *J. Phys. Chem. B*, **102**, 8201–8208.
Durham, B., Fairris, J. L., McLean, M., Millett, F., Scott, J. R., Sligar, S. G. & Willie, A. (1995). *J. Bioenerg. Biomembr.* **27**, 331–340.
Durley, R. C. E. & Mathews, F. S. (1996). *Acta Cryst.* D**52**, 65–76.
Feng, C., Kedia, R. V., Hazzard, J. T., Hurley, J. K., Tollin, G. & Enemark, J. H. (2002). *Biochemistry*, **41**, 5816–5821.

Funk, W. D., Lo, T. P., Mauk, M. R., Brayer, G. D., MacGillivray, R. T. & Mauk, A. G. (1990). *Biochemistry*, **23**, 5500–5508.
Guex, N. & Peitsch, M. C. (1997). *Electrophoresis*, **18**, 2714–2723.
Hille, R. (1996). *Chem. Rev.* **96**, 2757–2816.
Johnson, J. L. & Rajagopalan, K. V. (1976). *J. Clin. Invest.* **58**, 543–550.
Johnson, J. L. & Rajagopalan, K. V. (1977). *J. Biol. Chem.* **252**, 2017–2025.
Jones, T. A., Zou, J. Y., Cowan, S. W. & Kjeldgaard, M. (1991). *Acta Cryst.* A**47**, 110–119.
Kappler, U., Bennett, B., Rethmeier, J., Schwarz, G., Deutzmann, R., McEwan, A. G. & Dahl, C. (2000). *J. Biol. Chem.* **275**, 13202–13212.
Kisker, C., Schindelin, H., Pacheco, A., Wehbi, W. A., Garrett, R. M., Rajagopalan, K. V., Enemark, J. H. & Rees, D. C. (1997). *Cell*, **91**, 973–983.
Kisker, C., Schindelin, H. & Rees, D. C. (1997). *Annu. Rev. Biochem.* **66**, 233–267.
Kossiakoff, A. A., Randal, M., Guenot, J. & Eigenbrot, C. (1992). *Proteins*, **14**, 65–74.
Kraulis, P. J. (1991). *J. Appl. Cryst.* **24**, 946–950.
La Mar, G. N. & Walker, F. A. (1972). *J. Am. Chem. Soc.* **94**, 8607–8608.
Marcus, R. A. & Sutin, N. (1985). *Biochim. Biophys. Acta*, **811**, 265–322.
Merritt, E. A. (1999). *Acta Cryst.* D**55**, 1109–1117.
Merritt, E. A. & Bacon, D. J. (1997). *Methods Enzymol.* **277**, 505–524.
Murshudov, G., Vagin, A. & Dodson, E. (1997). *Acta Cryst.* D**53**, 240–255.
Navaza, J. (1994). *Acta Cryst.* A**50**, 157–163.
Nicholls, A., Sharp, K. A. & Honig, B. (1991). *Proteins*, **11**, 281–296.
Otwinowski, Z. & Minor, W. (1997). *Methods Enzymol.* **276**, 307–326.
Pacheco, A., Hazzard, J. T., Tollin, G. & Enemark, J. H. (1999). *J. Biol. Inorg. Chem.* **4**, 390–401.
Page, C. C., Moser, C. C., Chen, X. & Dutton, P. L. (1999). *Nature (London)*, **402**, 47–52.
Perrakis, A., Morris, R. M. & Lamzin, V. S. (1999). *Nature Struct. Biol.* **6**, 458–463.
Rees, D. C. (1985). *Proc. Natl Acad. Sci. USA*, **82**, 3082–3085.
Rivera, M., Seetharaman, R., Girdhar, D., Wirtz, M., Zhang, X., Wang, X. & White, S. (1998). *Biochemistry*, **37**, 1485–1494.
Sarma, S., Dangi, B., Yan, C., DiGate, R. J., Banville, D. L. & Guiles, R. D. (1997). *Biochemistry*, **36**, 5645–5657.
Temple, C. A. & Rajagopalan, K. V. (2000). *J. Biol. Chem.* **275**, 40202–40210.
Vergeres, G. & Waskell, L. (1995). *Biochimie*, **77**, 604–620.
Wu, J., Gan, J. H., Xia, Z. X., Wang, Y. H., Wang, W. H., Xue, L. L., Xie, Y. & Huang, Z. X. (2000). *Proteins*, **40**, 249–257.